

Effects of different growth conditions on epitaxial growth of (001) Ga_2O_3 films by MOCVD

Ke Qin(秦柯), Yun-Long He(何云龙), Zhan Wang(王湛), Jing Sun(孙静), Ying Zhou(周颖), Yang Liu(刘洋), Jin-Wei Liu(刘金炜) Zhuo-Wen Huang(黄卓文), Ji-Wei Jiang(江继伟), Zhu Jin(金竹), Hui Zhang(张辉), Xiao-Li Lu(陆小力), Xue-Feng Zheng(郑雪峰), Xiao-Hua Ma(马晓华), and Yue Hao(郝跃)

Citation: Chin. Phys. B, 2026, 35 (**4**): 048201. DOI: 10.1088/1674-1056/ae04cd
http://cpb.iphy.ac.cn; http://iopscience.iop.org/cpb

What follows is a list of articles you may be interested in

A high-sensitivity deep-junction single-photon detector for near-infrared imaging

Yuanhao Bi(毕元昊), Dajing Bian(卞大井), Ming Li(李铭), and Yue Xu(徐跃)
Chin. Phys. B, 2025, 34 (**6**): 068501. DOI: 10.1088/1674-1056/adc40b

Atmospheric neutron single event effects for multiple convolutional neural networks based on 28-nm and 16-nm SoC

Xu Zhao(赵旭), Xuecheng Du(杜雪成), Chao Ma(马超), Zhiliang Hu(胡志良), Weitao Yang(杨卫涛), and Bo Zheng(郑波)
Chin. Phys. B, 2025, 34 (**1**): 018501. DOI: 10.1088/1674-1056/ad8b38

Single event effects evaluation on convolution neural network in Xilinx 28 nm system on chip

Xu Zhao(赵旭), Xuecheng Du(杜雪成), Xu Xiong(熊旭), Chao Ma(马超), Weitao Yang(杨卫涛), Bo Zheng(郑波), and Chao Zhou(周超)
Chin. Phys. B, 2024, 33 (**7**): 078501. DOI: 10.1088/1674-1056/ad3b82

Near-infrared photocatalysis based on upconversion nanomaterials

Xingyuan Guo(郭星原), Zhe Wang(王哲), Shengyan Yin(尹升燕), and Weiping Qin(秦伟平)
Chin. Phys. B, 2022, 31 (**10**): 108201. DOI: 10.1088/1674-1056/ac7556

Synthesis of multi-walled carbon nanotubes using CoMnMgO catalysts through catalytic chemical vapor deposition

Yang Wen (杨文), Feng Yan-Yan (冯艳艳), Jiang Cheng-Fa (江成发), Chu Wei (储伟)
Chin. Phys. B, 2014, 23 (**12**): 128201. DOI: 10.1088/1674-1056/23/12/128201

Effects of different growth conditions on epitaxial growth of (001) Ga_2O_3 films by MOCVD

Ke Qin(秦柯)[1], Yun-Long He(何云龙)[1,3,†], Zhan Wang(王湛)[2,‡], Jing Sun(孙静)[1,3], Ying Zhou(周颖)[1], Yang Liu(刘洋)[1], Jin-Wei Liu(刘金炜)[1], Zhuo-Wen Huang(黄卓文)[1], Ji-Wei Jiang(江继伟)[4], Zhu Jin(金竹)[5], Hui Zhang(张辉)[4,5], Xiao-Li Lu(陆小力)[1], Xue-Feng Zheng(郑雪峰)[1], Xiao-Hua Ma(马晓华)[1], and Yue Hao(郝跃)[1]

[1] *State Key Laboratory of Wide-Bandgap Semiconductor Devices and Integrated Technology, National Engineering Research Center of Wide Band-gap Semiconductor, School of Microelectronics, Xidian University, Xi'an* 710071, *China*
[2] *School of Electronic Engineering, Xi'an University of Posts & Telecommunications, Xi'an* 710121, *China*
[3] *Guangzhou Institute of Technology, Xidian University, Guangzhou* 510555, *China*
[4] *Hangzhou Garen Semiconductor Co., Ltd., Hangzhou* 311200, *China*
[5] *State Key Laboratory of Silicon and Advanced Semiconductor Materials, School of Materials Science and Engineering, Zhejiang University, Hangzhou* 310027, *China*

(Received 15 July 2025; revised manuscript received 26 August 2025; accepted manuscript online 9 September 2025)

The β-Ga_2O_3 epitaxial thin films were grown on (001) β-Ga_2O_3 substrates using metalorganic chemical vapor deposition (MOCVD), and the effects of key growth parameters — including temperature, pressure, and oxygen-to-gallium ratio (O_2/Ga) — on the crystalline quality, surface morphology, and electrical properties of the films were systematically investigated. The results show that while variations in these parameters did not alter the (001) preferential orientation of the β-Ga_2O_3 films, they significantly influenced other properties. By optimizing the growth parameters, films with a surface roughness as low as 1.5 nm and the full width at half maximum (FWHM) of 33.7 arcsec were achieved. X-ray photoelectron spectroscopy (XPS) analysis showed that the oxygen vacancy concentration was significantly reduced under the optimized O_2/Ga ratio of 820. Schottky barrier diodes (SBDs) were fabricated from three different β-Ga_2O_3 films grown under distinct O_2/Ga ratios. The SBD fabricated under the optimized O_2/Ga ratio of 820, exhibits a low turn-on voltage of 0.5 V, low on-resistance of 0.022 m$\Omega\cdot$cm^2, and a high forward current density of 678.16 A/cm^2 at 3 V. These results provide essential material and theoretical foundations for the development of β-Ga_2O_3 based high-power electronic devices.

Keywords: β-Ga_2O_3, MOCVD, epitaxial layer, Schottky barrier diode

PACS: 82.45.Vp, 82.33.Ya, 85.30.De

DOI: 10.1088/1674-1056/ae04cd **CSTR:** 32038.14.CPB.ae04cd

1. Introduction

In recent years, monoclinic gallium oxide (β-Ga_2O_3) has demonstrated significant potential in power electronics due to its wide bandgap ($\sim$ 4.8 eV), high breakdown electric field ($\sim$8 MV/cm), and high Baliga's figure of merit ($\sim$ 3444).[1] Due to the absence of p-type doping technology, current research efforts primarily focus on unipolar Ga_2O_3 devices. β-Ga_2O_3-based SBDs and metal–oxide–semiconductor field-effect transistors (MOSFETs) have attracted considerable attention due to their potential for application in high power electronics systems. Currently, β-Ga_2O_3-based SBDs exhibit the highest power figure-of-merit (PFOM) value of 15.2 GW/cm^2,[2] approaching the theoretical limit. In contrast, the PFOM of β-Ga_2O_3-based MOSFETs remains at only 0.95 GW/cm^2,[3] and 0.73 GW/cm^2 of PFOM of enhancement-mode MOSFETs is even lower,[4] indicating a significant gap from the theoretical maximum values. This discrepancy is primarily attributed to differences in the epitaxial growth techniques employed: most β-Ga_2O_3 SBDs are fabricated using epitaxial films grown by hydride vapor phase epitaxy (HVPE), whereas MOSFETs typically rely on MOCVD. These results suggest that the quality of β-Ga_2O_3 epitaxial layers grown by MOCVD still requires substantial improvement.

Currently, β-Ga_2O_3 epitaxial processes can be categorized into homoepitaxy and heteroepitaxy.[5–7] Homoepitaxy includes four crystal orientations: (100), (010), (001), and (-201). In this study, the (001)-oriented β-Ga_2O_3 substrate was chosen primarily for two key reasons: it enables the cost-effective production of large-diameter commercial wafers,[8,9] and it is the most widely used orientation in power devices, particularly in vertical devices.[10] The (001) orientation offers superior surface morphology and reduced defect density, which are critical for enhancing device performance and reliability in power applications. Current epitaxial growth techniques for β-Ga_2O_3 include HVPE, MOCVD, mist-CVD, and

†Corresponding author. E-mail: ylhe@xidian.edu.cn
‡Corresponding author. E-mail: xdwangzhan@163.com

© 2026 Chinese Physical Society and IOP Publishing Ltd. All rights, including for text and data mining, AI training, and similar technologies, are reserved.

molecular beam epitaxy (MBE). Among these, HVPE, with its fast growth rate and tunable low-concentration doping, holds a significant market share. Nevertheless, HVPE growth at high rates often leads to pronounced surface roughness, characterized by surface steps and pits, which necessitates mechanical and chemical-mechanical polishing (CMP) prior to device fabrication.[11] These additional steps not only raise production costs but also carry the risk of introducing impurities or contaminants onto the surface during polishing. MOCVD, capable of large-scale epitaxy with competitive growth rates, is poised to dominate the future market for gallium oxide epitaxial materials.[12] However, the epitaxial growth of (001)-oriented thin films via MOCVD exhibits a narrow process window,[13] resulting in limited film quality. Therefore, further in-depth research of growth conditions remains necessary.

In this study, the influence of various growth parameters on the material properties of (001) β-Ga_2O_3 thin films using MOCVD were systematically investigated and the SBDs were fabricated for verification. Firstly, epitaxial growth was carried out by independently varying the growth temperature, pressure, and oxygen-to-gallium (O_2/Ga) ratio. The surface morphology and crystal quality of the films were characterized and analyzed using atomic force microscopy (AFM), scanning electron microscopy (SEM), x-ray diffraction (XRD), and x-ray photoelectron spectroscopy (XPS), allowing the determination of optimal growth conditions. Subsequently, β-Ga_2O_3-based SBDs were successfully fabricated using the optimized process parameters, and their electrical characteristics were evaluated to validate the epitaxial material. The findings of this study not only provide process guidelines for high quality β-Ga_2O_3 film growth but also establish an experimental foundation for the design and performance optimization of β-Ga_2O_3-based power devices.

2. Experiment and method

β-Ga_2O_3 thin films were epitaxially grown on (001)-oriented β-Ga_2O_3 substrates using MOCVD. Prior to loading into the reaction chamber, the substrates were sequentially ultrasonically cleaned in acetone and isopropanol, followed by 5 minutes deionized water rinse. Trimethylgallium (TMGa) and pure O_2 served as the Ga and O precursors, respectively, and argon (Ar) was used as the carrier gas. Both sapphire and β-Ga_2O_3 substrates were placed in the chamber simultaneously during growth. Based on the refractive index difference between sapphire and β-Ga_2O_3, *in-situ* reflectance monitoring was used to measure the growth rates of the β-Ga_2O_3 epitaxial layer in real time.[14] To investigate the effects of growth temperature and pressure on the material properties of (001) β-Ga_2O_3 films, five samples were prepared. Samples A–C were grown at 850 °C, 900 °C, and 950 °C, respectively, while maintaining other parameters constant. Subsequently, the pressure was varied to 100 mbar (1 bar = 10^5 Pa) and 150 mbar (samples D and E) while maintaining the optimal temperature. To enable device level verification, three additional Si-doped samples, designated as samples F, G, and H were fabricated, each with a target film thickness of 1 μm. These samples were prepared with varying O_2/Ga ratios. Detailed growth parameters are summarized in Table 1.

Table 1. Growth conditions of eight samples.

Sample No.	Temperature (°C)	Pressure (mbar)	O_2/Ga ratio	O_2 flow rate (sccm)	Carrier gas flow rate (sccm)	Total gas flow rate (sccm)
Sample A	850	50	820	4480	450	18000
Sample B	900	50	820	4480	450	18000
Sample C	950	50	820	4480	450	18000
Sample D	850	100	820	4480	450	18000
Sample E	850	150	820	4480	450	18000
Sample F	850	150	398	4480	900	18000
Sample G	850	150	820	4480	450	18000
Sample H	850	150	1200	4480	300	18000

β-Ga_2O_3 Schottky diodes were fabricated using samples F–H. The fabrication process started with ohmic contacts formed by an alloyed Ti/Au stack annealed at 470 °C for 1 min. Subsequently, the wafers were cleaned by sequential rinsing in acetone, ethanol, water, and finally dried with nitrogen. The anode electrode was formed by the Ni/Au electron beam evaporation and liftoff. Circular device structures are set in all devices, and the radius of the anode electrode is 60 μm. The cross-sectional schematic diagram in the insets of Fig. 6, which clearly labels all constituent layers and their corresponding materials.

3. Results and discussion

We first investigated the influence of growth temperature on film surface morphology and crystalline quality by preparing three samples (samples A–C) at 850 °C, 900 °C, and 950 °C, respectively, while keeping all other growth parameters constant. Presented in Fig. 1(a) are the XRD 2θ–ω scan patterns of β-Ga_2O_3 thin films grown on (001) β-Ga_2O_3 substrates at various temperatures. All films exhibit

high-intensity, distinct diffraction peaks corresponding to the (001) plane of β-Ga_2O_3, as well as an additional (-401) peak. The prominent (002) peak suggests that the preferred growth orientation is temperature-independent. The relatively weak intensity of the (-401) peak, compared to the (002) peak, indicates a small fraction of rotational domains. This minor structural feature does not compromise the dominance of the (001) orientation, thereby preserving the overall epitaxial quality, which is consistent with previous reports.[15,16] Displayed in Fig. 1(b) are the rocking curves corresponding to the (002) diffraction peak of the epitaxial films. The FWHM values for samples A–C are 35.7 arcsec, 34.8 arcsec, and 44.8 arcsec, respectively.

As the growth temperature increased to 950 °C (corresponding to sample C), the intensity of the (002) diffraction peak weakened, and the FWHM value significantly increased. This phenomenon can be attributed to two main mechanisms. First, higher temperatures enhance the thermal energy of reactant atoms, promoting their migration and rearrangement on the substrate surface.[17] While this facilitates tighter grain bonding, it may also lead to competition between layer-by-layer and island growth modes, reducing overall crystallinity, thus weakening the diffraction peak intensity and increasing FWHM. Second, higher temperatures may intensify the desorption of atoms or molecules from the substrate,[18] reducing the number of atoms available for film growth and introducing defects like oxygen vacancies. These defects disrupt the crystal's periodic arrangement, further decreasing diffraction peak intensity.

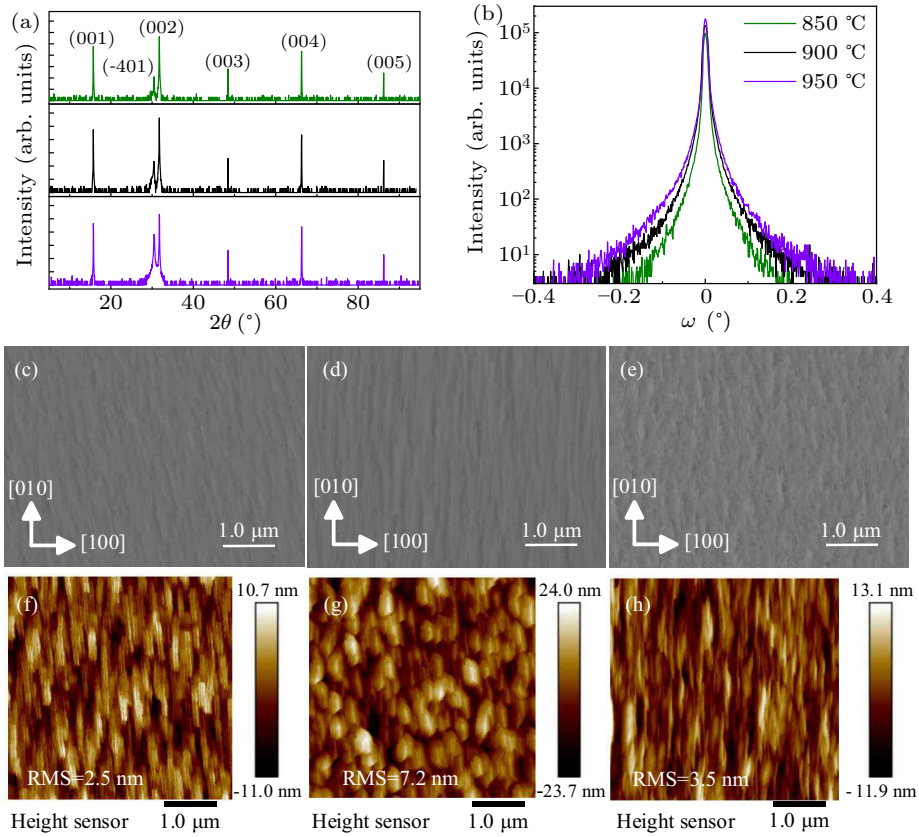


Fig. 1. (a) XRD 2θ–ω scans; (b) XRD ω scans; (c)–(e) corresponding SEM images (scale bar: 1 μm) with a coordinate system marking [010] and [100] crystallographic directions, and (f)–(h) corresponding AFM images (scan area: 5 μm×5 μm) of surface microstructures of Ga_2O_3 films grown at 850, 900, and 950 °C.

Additionally, the (002) peak position slightly shifted with temperature. According to the Bragg diffraction law:

$$2d\sin\theta = n\lambda, \tag{1}$$

where d is the interplanar spacing, θ is the grazing angle, λ is the wavelength, and n is the reflection order. The value of d increases with increasing temperature, which indicates that the strain caused by lattice mismatch and coefficients of thermal expansion decreases as the temperature increases.[19] This leads to minute adjustments in the interplanar spacing d, consequently affecting diffraction peak positions through the Bragg relation.

At growth temperatures of 850 °C, 900 °C, and 950 °C, the surface SEM images of (001) β-Ga_2O_3 films are presented in Figs. 1(c)–1(e), respectively. At 850 °C (sample A), the film surface exhibits shallow linear grooves along the [010] orientation, as indicated by the coordinate system in Fig. 1(c), but remains relatively smooth. As the temperature rises to 900 °C (sample B), the surface deteriorates significantly, with deeper grooves along [010]. At 950 °C (sample C), the surface shows

numerous grooves with unclear orientation. Figures 1(f)–1(h) present the AFM images of films grown at these temperatures. To quantify surface roughness, the root-mean-square roughness (RMS) was used for characterization. The RMS values obtained in this experiment at the three respective temperatures were 2.5 nm, 7.17 nm, and 3.5 nm.

At a growth temperature of 850 °C (sample A), the film surface displays a striped morphology while maintaining an overall flat profile. This suggests a stable growth process at this temperature, where the thermal motion of atoms is constrained, enabling them to settle into energetically favorable positions on the substrate. The orderly migration and arrangement of atoms on the surface minimize defect formation. When the temperature is elevated to 900 °C (sample B), the grain size increases, and the surface morphology has deteriorated obviously, characterized by the coexistence of two-dimensional growth and three-dimensional (3D) island-like structures. This behavior is associated with enhanced atomic diffusion, where the increased diffusion rate allows atoms to cross step edges more easily and promotes island formation.[20] Although the FWHM broadens at 950 °C, the simultaneous reduction in surface roughness can be rationalized. At this temperature, the higher energy of surface particles provides sufficient driving force for desorption and evaporation from the substrate, leading to smaller growth islands.[21] These islands tend to pack more uniformly, resulting in a smoother surface. The temperature-mediated growth mechanism is schematically presented in Fig. 2(a).

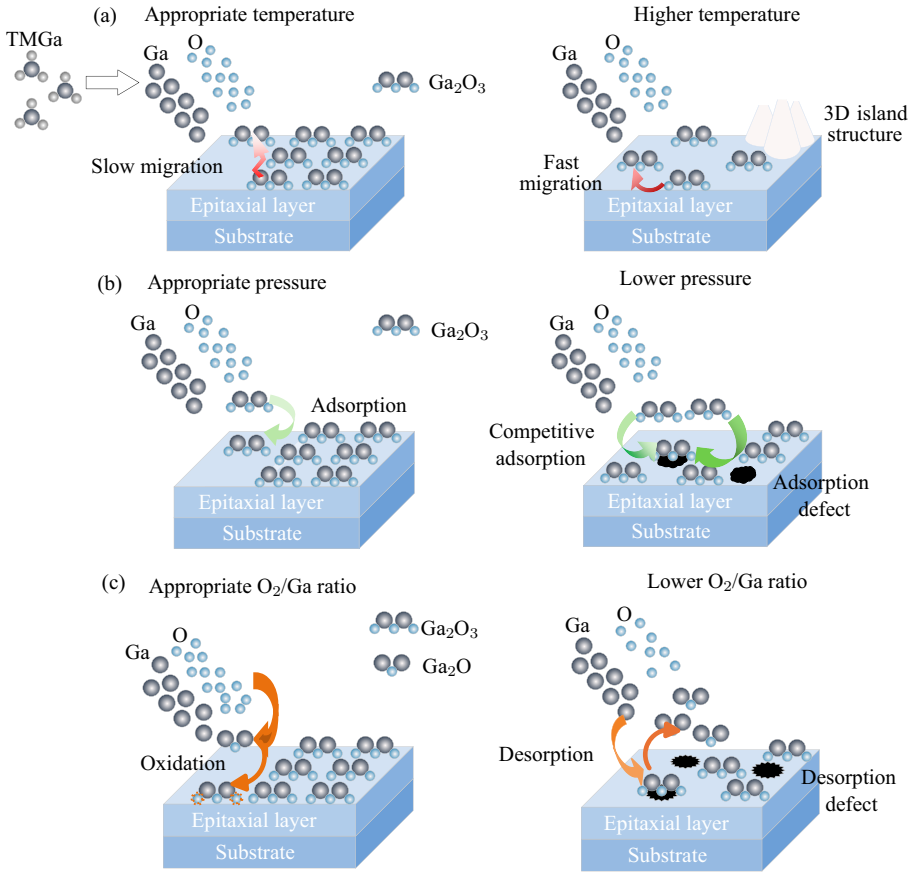


Fig. 2. (a) Schematic diagram of β-Ga_2O_3 epitaxy on (001) substrates at various temperatures (arrows show atomic migration), (b) schematic diagram of β-Ga_2O_3 epitaxy on (001) substrates at various pressures (arrows show atomic adsorption), and (c) schematic diagram of β-Ga_2O_3 epitaxy on (001) substrates at various O_2/Ga ratios.

An integrative evaluation of the XRD, SEM, and AFM data reveals that at 850 °C, the (002) diffraction peak is characterized by high intensity and a comparatively low FWHM, with the rocking curve exhibiting a symmetric configuration. Moreover, the surface roughness is notably reduced, and the surface morphology is remarkably planar. These findings show that this specific temperature condition is optimally suited for the epitaxial growth of β-Ga_2O_3 films.

The effect of chamber pressure on film characteristics was systematically examined by growing β-Ga_2O_3 films under three different pressures (50 mbar, 100 mbar, and 150 mbar), corresponding to samples A, D, and E, with all other parameters fixed (Table 1). XRD, SEM, and AFM were employed to analyze surface morphology and crystal quality, evaluating pressure's impact on film growth.

The XRD 2θ–ω scan spectra depicted in Fig. 3(a) correspond to β-Ga_2O_3 thin films epitaxially grown on (001) β-Ga_2O_3 substrates under various growth pressures. All films exhibit high-intensity, distinct diffraction peaks corresponding to the (001) plane of β-Ga_2O_3, along with an additional (-401)

peak. The prominent (002) peak suggests that increased pressure does not alter the preferred growth orientation. The rocking curves of the (002) diffraction peak for β-Ga_2O_3 epitaxial films are shown in Fig. 3(b). The FWHM values for samples A, D, and E are 35.7 arcsec, 30.6 arcsec, and 33.7 arcsec, respectively.

When the growth pressure was set to 50 mbar (corresponding to sample A), the intensity of the (002) diffraction peak decreased to about one-tenth of that at 150 mbar, while the FWHM indicates a higher threading dislocation (TD) density. This can be explained by the relationship between FWHM and dislocation density[22]

$$D = \frac{B^2}{2\ln 2\pi b^2}, \tag{2}$$

where B is the diffraction peak FWHM, D is the dislocation density, and b is the Burgers vector. The results indicate a high density of dislocations, which degrades the overall film quality. When the pressure is increased to 100 mbar (sample D), the intensity of the (002) diffraction peak nearly matches that at 150 mbar (sample E), but the (-401) peak becomes unusually prominent. This additional peak is attributed to crystal rotation from the [001] to the [-401] direction, which redistributes surface energy, promotes strain accumulation, and leads to premature termination of [001] epitaxial growth.[23] For high-quality film growth, however, a strong (-401) peak is undesirable. In contrast, at 150 mbar, the intensity of the (002) diffraction peak reaches a high level, while the intensity of the (-401) additional peak is relatively weak. Moreover, the FWHM value remains at a relatively low level. This indicates that under this pressure condition, the film has fewer defects and dislocations, along with good crystallinity.

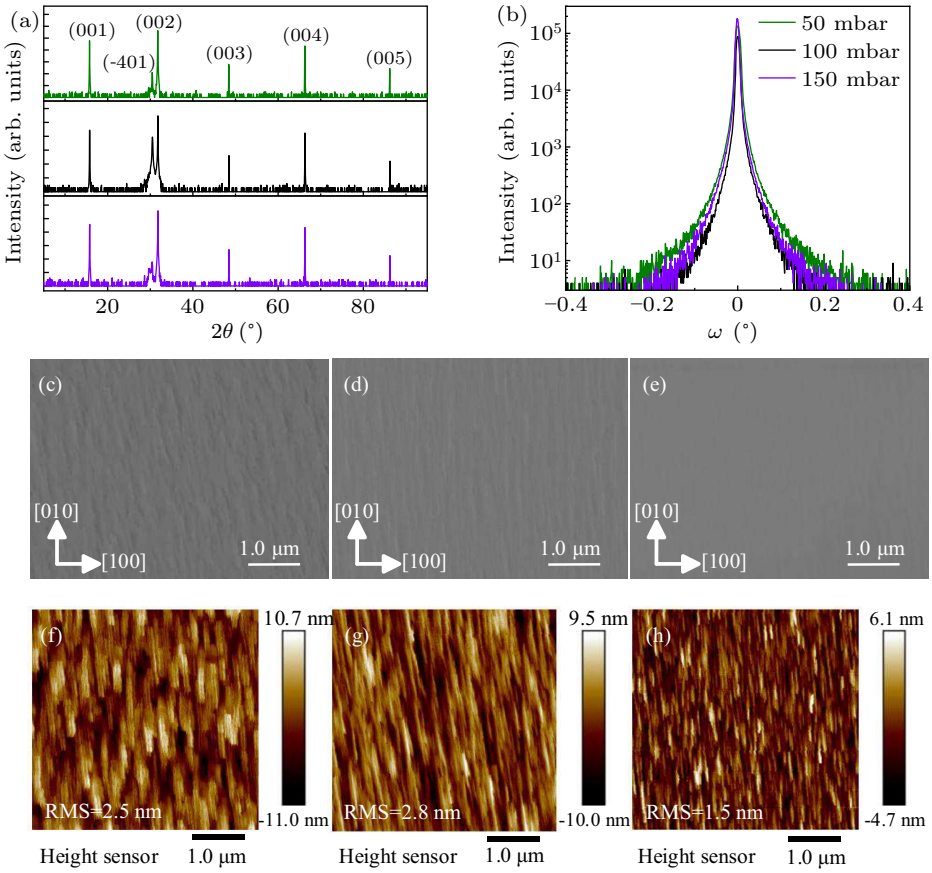


Fig. 3. (a) XRD 2θ–ω scans, (b) XRD ω scans, (c)–(e) corresponding SEM images (scale bar: 1 μm) with a coordinate system marking [010] and [100] crystallographic directions, and (f)–(h) corresponding AFM images (scan area: 5 μm×5 μm) of surface microstructures of Ga_2O_3 films grown at 50 mbar, 100 mbar, and 150 mbar.

Figures 3(c)–3(e) present the surface SEM images of (001) β-Ga_2O_3 films grown under pressures of 50 mbar, 100 mbar, and 150 mbar, respectively. At 50 mbar (sample A), the surface exhibits distinct fine linear undulations along the [010] orientation. As the pressure increases to 100 mbar (sample D), these linear grooves become denser, and at 150 mbar (sample E), the surface transitions from fine linear grooves to a smoother morphology.

The surface AFM images of films grown under different pressures are illustrated in Figs. 3(f)–3(h). At 50 mbar (sample A), the film surface exhibits a rough and irregular stripe-like structure, which may be influenced by factors such as deposition rate, precursor diffusion behavior, and surface energy minimization mechanisms. In terms of growth rate, a value of 1.040 μm/h was measured at this pressure, which may also contribute to the observed surface morphology. How-

ever, the exact cause of the surface morphology remains unclear from these observations alone. As the pressure increases to 100 mbar (sample D), the surface exhibits fine and sharp stripe-like protrusions with enhanced regularity. This phenomenon is associated with the formation of a thick boundary layer, where the reduced mean free path of gas molecules leads to its thickening. The thicker boundary layer hinders the diffusion of Ga precursor and other reactants toward the substrate, limiting surface atom diffusion rate and suppressing lateral growth on the surface.[24] As a result, atoms cannot rearrange efficiently into an ordered lattice, while the uneven reactant distribution across the surface leads to local variations in growth rates and further increases surface roughness.[25] Meanwhile, the growth rate decreases to 0.971 μm/h. This slowed growth rate likely causes precursor accumulation in localized regions, forming finer and sharper stripe-like protrusions and increasing surface roughness. These effects are consistent with observations in the literature, where a thicker boundary layer leads to degraded surface quality under high-pressure conditions.[26] When the pressure reaches 150 mbar (sample E), the surface morphology changes again, nearly merging into nano-stripe structures. This phenomenon can be attributed to pressure-dependent thin-film growth kinetics: At lower pressures, the higher deposition rate results in insufficient surface migration time for adatoms, leading to competitive occupation of adsorption sites by multiple atoms and thus promoting defect formation.[27] In contrast, at 150 mbar, where the growth rate is measured at 0.587 μm/h, the reduced growth rate allows adatoms to achieve enhanced surface diffusion, resulting in decreased film roughness and refined grain size.[28] The pressure-mediated growth mechanisms are schematically presented in Fig. 2(b).

Comprehensive analysis of XRD, SEM, and AFM results reveals that at 150 mbar, the (002) diffraction peak exhibits high intensity and a narrow FWHM, with low surface roughness and a flat morphology, facilitating ordered crystal arrangement and high-quality crystallization while effectively suppressing unfavorable crystal domain rotation. Thus, 150 mbar is optimal for high-quality β-Ga_2O_3 film formation among the tested conditions.

To enable fabrication of β-Ga_2O_3 Schottky barrier diodes, we grew a 1-μm-thick Si-doped epitaxial layer under the same growth conditions as sample E, but with extended growth time and Si incorporation ($\sim 9\times10^{17}$ cm^{-3}), and obtained sample G. Furthermore, to investigate the influence of the O_2/Ga ratio on (001)-oriented epitaxial growth, we maintained a constant O_2 flow rate of 4480 sccm while adjusting the TMGa flow to achieve O_2/Ga ratios of 398 and 1200, corresponding to samples F and H, respectively. XRD, SEM, AFM, and XPS were employed to analyze surface morphology and crystal quality, evaluating the impact of O_2/Ga ratios on film growth.

The XRD 2θ–ω scan patterns of β-Ga_2O_3 films deposited on (001) β-Ga_2O_3 substrates with different O_2/Ga ratios are displayed in Fig. 4(a). All films exhibit high-intensity, distinct diffraction peaks corresponding to the (001) plane of β-Ga_2O_3, along with additional peaks at (-401) and (-311),[29] indicating uniform epitaxial growth and the exclusive presence of the β-phase. Notably, while films grown under short growth durations (e.g., sample E, 600 s, undoped) did not exhibit the (-311) reflection, the long-duration film (sample G, 3000 s, Si-doped at 9×10^{17} cm^{-3}) clearly showed this peak. Considering that the Si concentration is about two orders of magnitude below the thresholds reported to alter orientation or induce amorphization in β-Ga_2O_3 ($\geq 10^{19}$ cm^{-3}–10^{20} cm^{-3}),[30] the emergence of the (-311) peak is attributed primarily to the prolonged growth time rather than to Si incorporation. This interpretation is consistent with previous studies. Terohid *et al.*[31] observed that extended growth durations enhance crystallinity and introduce additional Bragg peaks, indicative of polycrystallinity. Moreover, the competitive texture evolution model proposed by Van der Drift[32] suggests that multiple orientations nucleate during the early stage of growth, while longer growth allows minor orientations to persist locally and become detectable in XRD. Taken together, our results demonstrate that the appearance of the (-311) peak originates from time-dependent competitive orientation evolution, rather than from Si doping effects. However, the specific underlying mechanism governing the formation of the (-311) peak still requires further investigation to clarify its full origin. Furthermore, the crystalline quality of these films was evaluated by rocking curve measurements, as shown in Fig. 4(b). The FWHM values for samples F–H are 64.2 arcsec, 56.5 arcsec, and 73.2 arcsec, respectively.

At an O_2/Ga ratio of 820 (corresponding to sample G), the FWHM reaches its minimum, indicating that the crystallinity and film quality are better at this condition. During growth, O_2 flow is constant. The lower O_2/Ga ratio implies insufficient oxygen relative to gallium, leading to oxygen vacancies (V_O) in the lattice, represented by the defect reaction

$$O_{lattice} \rightarrow V_O + O_{free}. \tag{3}$$

These vacancies disrupt the lattice structure of the film and reduce crystallinity. Conversely, excessive oxygen partial pressure results in interstitial oxygen incorporation, which perturb the β-Ga_2O_3 crystal structure and facilitate polycrystalline phase formation.[33]

Displayed in Figs. 4(c)–4(e) are the surface SEM images of (001) β-Ga_2O_3 films grown at O_2/Ga ratios of 398, 820,

and 1200, respectively. At a ratio of 398 (sample F), the surface morphology deteriorates significantly, with fine linear undulations along [010] transforming into larger, irregular wavy stripes. This change can be attributed to oxygen deficiency under Ga-rich conditions, where enhanced β-Ga_2O_3 desorption reduces Ga adatom diffusion and favors random nucleation and island growth, leading to increased surface roughness.[34] Furthermore, at an O_2/Ga ratio of 820 (sample G), the fine linear undulations along the [010] crystal direction become more pronounced, with a slight increase in amplitude. This change shows that under the optimal O_2/Ga conditions, the film can form a more orderly and clearly oriented structure. However, at an O_2/Ga ratio of 1200 (sample H), the film surface appears smooth, yet linear undulations along the [010] direction are visible, attributed to the formation of (100) facets during growth.[35] Although the surface is smoother, excess oxygen increases adatom diffusion but simultaneously introduces interstitial oxygen, disturbing crystalline order.

Displayed in Figs. 4(f)–4(h) are the surface AFM images of (001) β-Ga_2O_3 films, which were grown under O_2/Ga ratios of 398, 820, and 1200, respectively. At a ratio of 398 (sample F), the surface of the film has uneven bumps or grooves, resulting from competitive desorption of suboxide Ga_2O during film growth. The corresponding reaction is

$$2\mathrm{Ga}(l) + \frac{3}{2}\mathrm{O_2}(g) \rightarrow \mathrm{Ga_2O_3}(s), \tag{4}$$

$$4\mathrm{Ga}(l) + \mathrm{Ga_2O_3}(s) \rightarrow 3\mathrm{Ga_2O}(g). \tag{5}$$

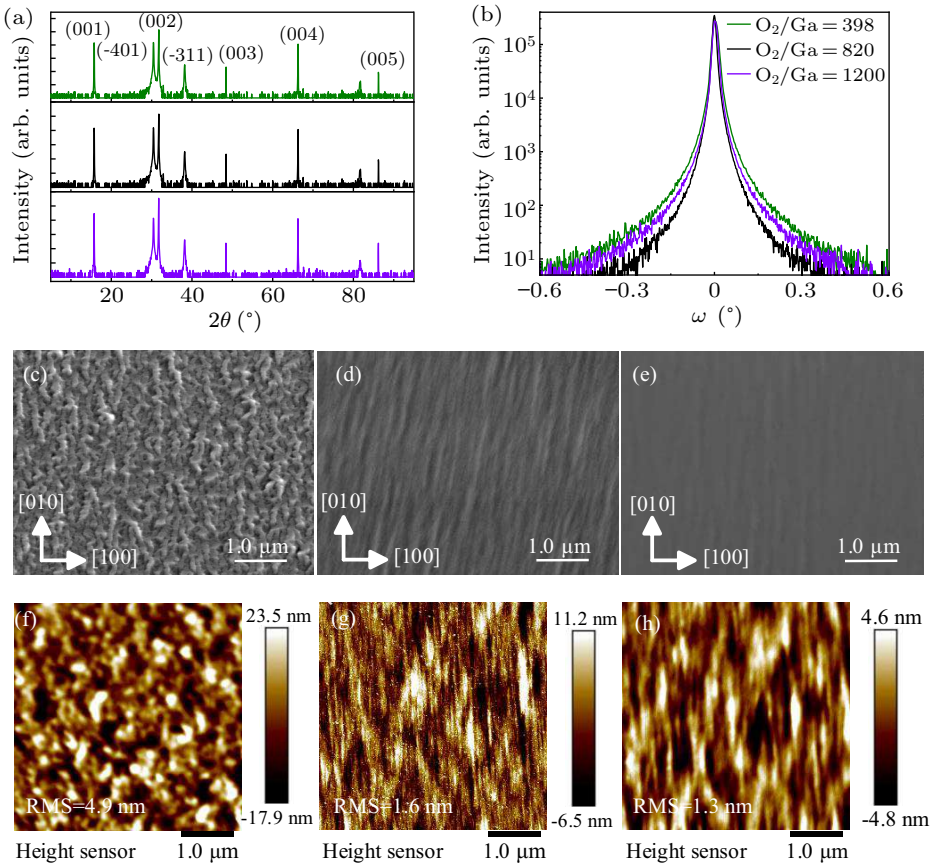


Fig. 4. (a) XRD 2θ–ω scans; (b) XRD ω scans; (c)–(e) corresponding SEM images (scale bar: 1 μm) with a coordinate system marking [010] and [100] crystallographic directions, and (f)–(h) corresponding AFM images (scan area: 5 μm×5 μm) of surface microstructures of Ga_2O_3 films grown at O_2/Ga ratios of 398, 820, and 1200.

When the O_2/Ga ratio is low, insufficient oxygen supply enhances the desorption reaction of Ga_2O, leading to the rearrangement of surface atoms and changes in surface morphology.[36] In contrast, when the O_2/Ga ratio is set to 820 or 1200, the film surface appears relatively smooth with reduced roughness. The O_2/Ga ratio-mediated growth mechanisms are schematically presented in Fig. 2(c). However, at an O_2/Ga ratio of 1200, although the surface is smooth, the grain height decreases. This is attributed to excess oxygen reducing adatom diffusion rate on the substrate surface,[37] which limits vertical grain growth. While this lowers surface roughness, it may also adversely affect other film properties.

XPS measurements were carried out to investigate the chemical information of the β-Ga_2O_3 films. Figure 5(a) displays the O 1s XPS spectra of β-Ga_2O_3 films grown at O_2/Ga ratios of 398, 820, and 1200 (samples F, G, and H). The O 1s peak is deconvoluted into two components, OI and OII, using Gaussian fitting. The OI peak corresponds to Ga–O bonds, while OII is associated with oxygen vacancies.[38] The OII/(OI+OII) ratio is used to estimate oxygen vacan-

cies. Sample F exhibits the highest ratio (31.52%), consistent with its lowest crystallinity. For sample G, the ratio drops to 10.62%, indicating reduced oxygen vacancies and improved crystallinity. Sample H shows a moderate increase to 17.28%, suggesting that excess oxygen introduces other defects (e.g., interstitial oxygen atoms) that limit further crystallinity improvement.

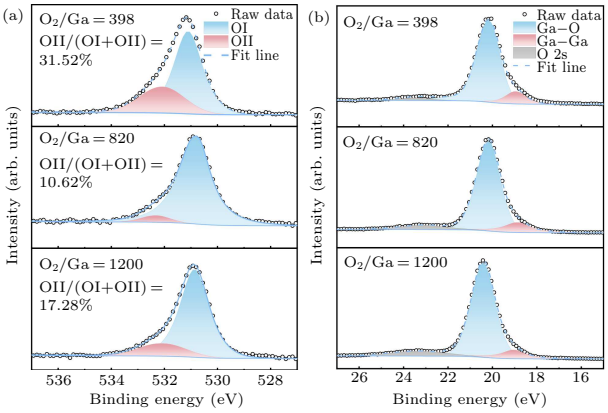


Fig. 5. XPS spectra and related analysis of β-Ga_2O_3 grown at O_2/Ga ratios of 398, 820, and 1200: (a) O 1s peaks, (b) Ga 3d peaks.

Figure 5(b) presents XPS spectra of the three samples in the Ga 3d peak. Besides the O 2s peak, two distinct peaks are observed, corresponding to Ga–O bonds (Ga_2O_3) and Ga–Ga bonds (Ga_2O).[39] Notably, the Ga–Ga bond signal is strongest in sample F, confirming severe oxygen deficiency at low O_2/Ga ratio. Sample G shows a decrease in Ga–Ga bonds, reflecting reduced Ga_2O formation and enhanced crystallinity. In contrast, sample H still contains a greater amount of Ga–Ga bonds, and this feature limits further improvement in its crystallinity compared to sample G.

Comprehensive analysis of the XRD, SEM, AFM, and XPS results indicates that when the O_2/Ga ratio is 820, the FWHM value is minimal, the surface roughness is low, and the relative content of oxygen vacancies is significantly reduced, suggesting superior crystallinity and film quality. Therefore, an O_2/Ga ratio of 820 is most favorable for film growth.

To comprehensively evaluate the material properties in functional devices, we fabricated Schottky barrier diodes using β-Ga_2O_3 films grown under three distinct O_2/Ga ratios (samples F–H, see Table 1 for growth parameters). Systematic characterization of device performance metrics (carrier concentration, on-resistance, and turn-on voltage, quantified in Table 2) provided direct evidence that the O_2/Ga ratio governs the crystalline quality of (001) β-Ga_2O_3 films, as revealed by structure-property correlations.

Table 2. Electrical parameters of SBDs.

Device No.	O_2/Ga ratio	Carrier concentration (cm^{-3})	Built-in potential (V)	On-resistance ($m\Omega\cdot cm^2$)	Current density (A/cm^2)-3 V	Turn-on voltage (V)	Ideality factor
F	398	4.5084×10^{17}	0.0515	0.1076	880.75	0.25	1.41
G	820	2.1366×10^{17}	0.1066	0.02249	678.16	0.57	1.03
H	1200	2.4545×10^{17}	0.0852	0.05409	22.66	2.5	1.21

Shown in Figs. 6(a)–6(c) are the $(1/C^2)$ *versus* applied voltage V curves at varying O_2/Ga ratios. The doping concentration and built-in potential (V_{bi}) of the SBD can be determined from the slope and x-intercept of the curves and applying the following formula:[40]

$$C = \frac{A\varepsilon_s}{W} = A\sqrt{\frac{q\varepsilon_s N_D}{2(V_{bi}-V)}}, \tag{6}$$

$$\frac{1}{C^2} = \frac{2(V_{bi}-V)}{A^2 q\varepsilon_s N_D}, \tag{7}$$

where A is the diode active area, ε_s is the β-Ga_2O_3 semiconductor permittivity, W is the depletion width, q is the electronic charge, N_D is the doping density, V_{bi} is the built-in potential, and V is the voltage applied.

The V_{bi} is related to the charge density in the space charge region. A higher carrier concentration increases the charge density in this region, which weakens the V_{bi}. At an O_2/Ga ratio of 398 (corresponding to device F), the lower ratio may lead to an insufficient oxygen supply, introducing more defects in β-Ga_2O_3 films.[41] These defects increase the carrier concentration, but when excessive, they scatter carriers and lower mobility, resulting in a lower V_{bi}. The smaller V_{bi} weakens the electric field, potentially affecting the device switching speed and breakdown voltage. At an intermediate O_2/Ga ratio of 820 (device G), a balance is achieved between carrier concentration and defect density, yielding the highest V_{bi} and improved film quality. In contrast, at an O_2/Ga ratio of 1200 (device H), the highest carrier concentration is observed, which may result from oxygen-related lattice defects such as interstitial oxygen.[42] These defects can introduce lattice stress, leading to cracks or fractures and reducing the mechanical strength of the films.

As shown in the insets of Figs. 6(a)–6(c), the variation of carrier concentration with depth is depicted. In all three graphs, the carrier concentration rapidly decreases within the initial 0.05 μm, indicating a transition from a highly doped region to a low-doped region. Notably, the inset in Fig. 6(b) demonstrates an ideal decline, where the carrier concentration stabilizes and maintains a relatively flat doping profile

across the remaining film depth. This suggests a stable incorporation of dopants during growth, achieving uniform doping distribution.[43]

Shown in Figs. 6(d)–6(f) are the rectifying behavior exhibited by all samples. Current varies linearly at a low bias ($V < 1$ V) in semi-log plots, deviating at a higher bias ($V > 1$ V). Forward bias J–V characteristics were analyzed using the thermionic emission (TE) model, yielding the current density[44]

$$J = J_{\mathrm{s}}\left[\exp\left(\frac{qV}{\eta kT}\right) - 1\right], \tag{8}$$

$$J_{\mathrm{s}} = A^{*}T^{2}\left(\frac{q\phi_{\mathrm{B}}}{\mathrm{e}^{\eta kT}}\right). \tag{9}$$

Here, J_{S} is the saturation current density, η is the ideality factor, V is the forward bias voltage, T is the absolute temperature, q is the electron charge, k is the Boltzmann constant, ϕ_{B} is the apparent Schottky barrier height (SBH), A is the effective diode area, and A^{*} is the effective Richardson constant, calculated to be 41.04 A·cm^{-2}·T^{-2}.

The η was extracted from the slope of the semi-log forward J–V curve using the linearized form of Eq. (8)

$$\eta = \frac{q}{kT}\frac{1}{\frac{\mathrm{d}(\ln J)}{\mathrm{d}V}}. \tag{10}$$

The η reflects the quality of the metal–semiconductor interface and the dominant transport mechanism; ideally it should be 1, but in practice deviations arise from interface states, barrier inhomogeneity, or defect-assisted transport.[45] The extracted η values (shown in Table 2) confirm that the value at an O_2/Ga ratio of 820 is closest to unity (1.03), indicating optimized growth and better interface quality.

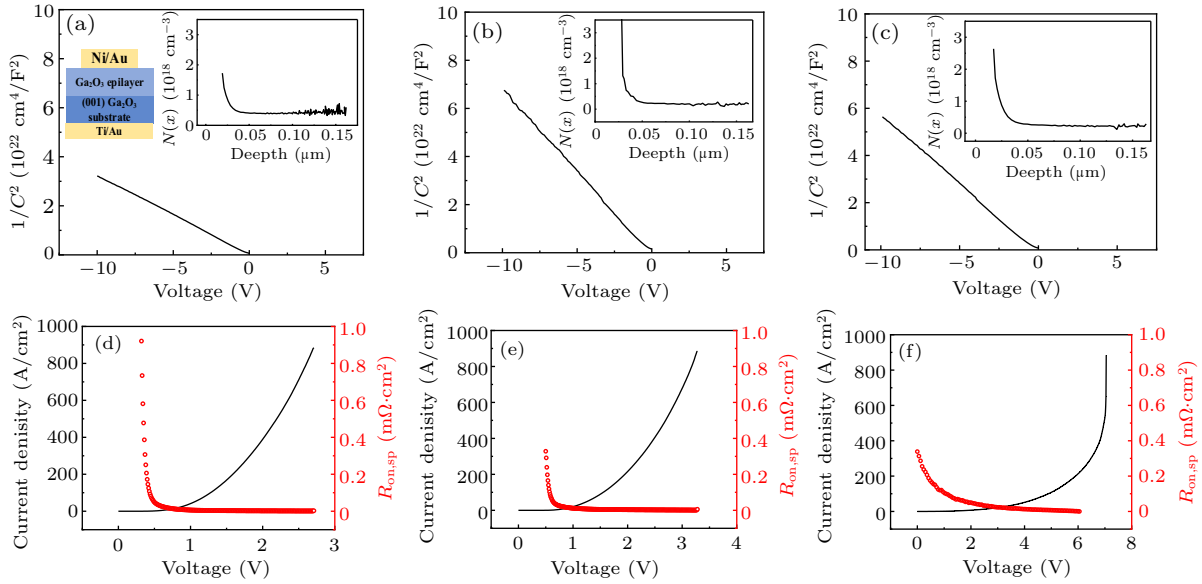


Fig. 6. (a)–(c) $(1/C^2)$–V characteristics of the Ga_2O_3 SBDs, the inset of each figure shows the variation of carrier concentration with depth; (d)–(f) the black curve is the J–V properties curve, and the red curve is the curve of the on-resistance changing with the voltage, the inset of (a) is the cross-section schematic diagram of the SBDs.

Additionally, the on-resistance ($R_{\mathrm{on,sp}}$) of the device was calculated using the following equation:[46]

$$R_{\mathrm{on,sp}} = R_{\mathrm{on}} \times A = \frac{\mathrm{d}V}{\mathrm{d}I} \times A = \frac{\mathrm{d}V}{\mathrm{d}J}, \tag{11}$$

where $R_{\mathrm{on,sp}}$ denotes the on-resistance, A represents the device anode area, and J signifies the current density. The extracted $R_{\mathrm{on,sp}}$ values for devices F, G, and H are summarized in Table 2, showing the lowest resistance at an O_2/Ga ratio of 820.

The results indicate that at an O_2/Ga ratio of 1200 (device H), the SBD exhibits the highest turn-on voltage (2.5 V) and the lowest forward current density (22.66 A/cm^2 at 3 V) among the three tested conditions. This behavior can be attributed to the excessive oxygen supply, which promotes Ga–O bond formation and leads to a widened optical bandgap.[47] Consequently, the Schottky barrier height increases, reducing forward current density. At an O_2/Ga ratio of 398, the Schottky diode exhibited the highest specific $R_{\mathrm{on,sp}}$ (0.11 mΩ·cm^2), which can be attributed to increased surface roughness. The enhanced surface morphological irregularities lead to current spreading effects, resulting in a larger effective conduction area.[48] When the O_2/Ga ratio is 820, the Schottky diode demonstrates a lower turn-on voltage (0.5 V), reduced $R_{\mathrm{on,sp}}$ (0.022 mΩ·cm^2), and a higher forward current density (678.16 A/cm^2 at 3 V), indicating superior electrical performance. This makes it particularly advantageous for applications requiring low-voltage operation, high efficiency, and high current handling capabilities.

A comprehensive analysis of the SBD's C–V and J–V characteristics, on-resistance, and turn-on voltage reveals that

at an O_2/Ga ratio of 820, the device exhibits lower background carrier concentration, higher built-in potential, lower on-resistance, and greater current density. Combined with the material properties of the thin film, this condition is optimal for film growth.

4. Conclusion and perspectives

In conclusion, this study systematically investigated the influence of key growth parameters, including growth temperature, chamber pressure, and O_2/Ga ratio, on the crystallinity and surface morphology of (001) β-Ga_2O_3 films grown by MOCVD. The results indicate that β-Ga_2O_3 films grown at a temperature of 850 °C, a pressure of 150 mbar, and an O_2/Ga ratio of 820 exhibit excellent crystallinity and surface smoothness. XRD analysis reveals a narrow FWHM value, indicating high crystal quality, while SEM and AFM further confirm a significant reduction in surface roughness. Specifically, the film exhibited a surface roughness of 1.5 nm, an FWHM of 33.7 arcsec, and a thickness of approximately 1 μm. The XPS analysis revealed a significant reduction in the oxygen vacancy concentration under the optimized O_2/Ga ratio of 820. SBDs were fabricated using β-Ga_2O_3 films grown under different O_2/Ga ratios, and their J–V characteristics were comparatively evaluated. The β-Ga_2O_3 film grown with an O_2/Ga ratio of 820 demonstrated the most favorable material properties and superior device performance. The corresponding SBD device showed a low turn-on voltage of 0.5 V, a low $R_{on,sp}$ of 0.022 mΩ·cm^2, and a high forward current density of 678.16 A/cm^2 at 3 V, along with the most uniform carrier concentration distribution. These findings lay the groundwork for both the material and theoretical development for the development of β-Ga_2O_3 based high-power electronic devices.

Acknowledgements

Project supported by the National Natural Science Foundation of China (Grant Nos. 62474133, U2241220, and 62304172), the Guangdong Basic and Applied Basic Research Foundation (Grant Nos. 2025A1515011176 and 2021A1515110020), the Opening Project of State Key Laboratory of Wide Bandgap Semiconductor Devices and Integrated Technology (Grant No. 2413S111), and the Fundamental Research Funds for the Central Universities of China (Grant No. ZDRC2002).

References

[1] Liao Z Y, Fang P W, Lu X, Wang G and Pei Y L 2025 *Chin. Phys. B* **34** 067304
[2] Li J S, Wan H H, Chiang C C, Yoo T J, Yu M H, Ren F, Kim H, Liao Y T and Pearton S J 2024 *ECS J. Solid State Sci. Technol.* **13** 035003
[3] Hendricks N S, Farzana E, Islam A E, Leedy K D, Liddy K J, Williams J, Dryden D M, Adams A M, Speck J S, Chabak K D and Green A J 2023 *Appl. Phys. Express* **16** 071002
[4] Wang X C, Lu X L, He Y L, Liu P, Shao Y, Li J N, Yang Y T, Li Y, Hao Y and Ma X H 2023 *35th International Symposium on Power Semiconductor Devices and ICs (ISPSD)* (Hong Kong: IEEE) pp. 390–393
[5] Zhang G, Wang Z Y, Chen S W, Xi Z Y, Wu C, Hu H Z, Liu Z, Wu F M, Wang S L, Fang Z L, Tang W H and Guo D Y 2025 *Laser Photon. Rev.* **19** e00255
[6] Wu G, Chen K, Ni Y Z, Wu C, Liu J S, Hu H Z, Zhang X H, Wang S L, Wu F M, Wu Z Y and Guo D Y 2025 *Mater. Today Phys.* **53** 101702
[7] Li J Y, Chen K, Wu C, Wu F M, Li S, Wu Z Y, Tang W H, Fang Z L and Guo D Y 2025 *Appl. Phys. Lett.* **126** 222104
[8] Gogova D, Ghezellou M, Tran D Q, Richter S, Papamichail A, Hassan J U, Persson A R, Persson P O Å, Kordina O, Monemar B, Hilfiker M, Schubert M, Paskov P P and Darakchieva V 2022 *AIP Adv.* **12** 055022
[9] Hernandez A, Islam M M, Saddatkia P, Codding C, Dulal P, Agarwal S, Janover A, Novak S, Huang M, Dang T, Snure M and Selim F A 2021 *Results Phys.* **25** 104167
[10] Liu Y, He Y L, Chen G R, Lu X L, Zheng X F, Ma X H and Hao Y 2025 *Res. Prog. Solid State Electron.* **45** 010101 (in Chinese)
[11] Higashiwaki M, Konishi K, Sasaki K, Goto K, Nomura K, Thieu Q T, Togashi R, Murakami H, Kumagai Y, Monemar B, Koukitu A, Kuramata A and Yamakoshi S 2016 *Appl. Phys. Lett.* **108** 133503
[12] Baldini M, Albrecht M, Fiedler A, Irmscher K, Schewski R and Wagner G 2017 *ECS J. Solid State Sci. Technol.* **6** Q3040
[13] Xu H J, Weng Y X, Chen K, Wu C, Hu H Z and Guo D Y 2025 *Adv. Opt. Mater.* **13** 2402238
[14] Chou T S, Bin Anooz S, Grüneberg R, Rehm J, Akhtar A, Mukherjee D, Petrik P and Popp A 2024 *Appl. Surf. Sci.* **652** 159370
[15] He Y L, Liu Y, Lu X L, Wang Z, Song X Q, Zhou Y, Zheng X F, Ma X H and Hao Y 2025 *J. Materiomics* **11** 100981
[16] Song X Q, He Y L, Wang Z, Lu X L, Sun J, Zhou Y, Liu Y, Fan J T, He X N, Zheng X F, Ma X H and Hao Y 2025 *Sci. China Mater.* **68** 515
[17] Zhang T, Li Y F, Zhang Y C, Feng Q, Ning J, Zhang C F, Zhang J C and Hao Y 2020 *ECS J. Solid State Sci. Technol.* **9** 065009
[18] Wang S 2022 *Fabrication of gallium oxide film on sapphire and its photo-electronic response research*, MS Thesis (Jinan: Shandong University) (in Chinese)
[19] Zhang T, Li Y F, Zhang Y C, Feng Q, Ning J, Zhang C F, Zhang J C and Hao Y 2021 *J. Alloys Compd.* **859** 157810
[20] Feng Z, Anhar Uddin Bhuiyan A F M, Karim M R and Zhao H 2019 *Appl. Phys. Lett.* **114** 250601
[21] Vogt P and Bierwagen O 2016 *Appl. Phys. Lett.* **108** 072101
[22] Zhao C L, Jiao T, Chen W, Li Z M, Dong X, Li Z D, Diao Z T, Zhang Y T, Zhang B L and Du G T 2022 *Coatings* **12** 645
[23] Meng L Y, Yu D S, Huang H L, Chae C, Hwang J and Zhao H 2024 *Cryst. Growth Des.* **24** 3737
[24] Bin Anooz S, Grüneberg R, Chou T S, Fiedler A, Irmscher K, Wouters C, Schewski R, Albrecht M, Galazka Z, Miller W, Schwarzkopf J and Popp A 2021 *J. Phys. Appl. Phys.* **54** 034003
[25] Biira S, Alawad B A B, Bissett H, Nel J T, Ntsoane T P, Hlatshwayo T T, Crouse P L and Malherbe J B 2017 *Ceram. Int.* **43** 1354
[26] Wu C C, Wuu D S, Lin P R, Chen T N and Horng R H 2009 *Nanoscale Res. Lett.* **4** 377
[27] Wang J, Luo T C, He Y C and Wang G 2023 *J. Cryst. Growth* **618** 127311
[28] Zhang T, Li Y F, Feng Q, Zhang Y C, Ning J, Zhang C F, Zhang J C and Hao Y 2021 *Mater. Sci. Semicond. Process.* **123** 105572
[29] Li X H, Zhang M, Yang J, Xing S, Gao Y, Li Y Z, Li S Y and Wang C J 2022 *Acta Phys. Sin.* **71** 048501 (in Chinese)
[30] Zhan J J, Wu Y, Zeng X H, Feng B Y, He M H, He G H and Ding S N 2024 *J. Appl. Phys.* **135** 105103
[31] Terohid S A A, Heidari S, Jafari A and Asgary S 2018 *Appl. Phys. A* **124** 56
[32] Van der Drift A 1967 *Philips Res. Repts* **22** 267
[33] Guo D Y, Wu Z P, Li P, An Y H, Liu H, Guo X C, Yan H, Wang G F, Sun C L, Li L H and Tang W H 2014 *Opt. Mater. Express* **4** 1067
[34] Tang W B, Han X L, Zhang X D, Li B T, Ma Y J, Zhang L, Chen T W, Zhou X, Bian C X, Hu Y, Chen D Y, Qi H J, Zeng Z M and Zhang B S 2023 *J. Semicond.* **44** 062801

[35] Tang W B 2023 *Homoepitaxial growth of β-Ga_2O_3 films and fabcration of schottky barrier diodes*, Ph. D. Dissertation (Hefei: University of Science and Technology of China) (in Chinese)

[36] Tang W B, Ma Y J, Zhang X D, Zhou X, Zhang L, Zhang X, Chen T W, Wei X, Lin W K, Mudiyanselage D H, Fu H Q and Zhang B S 2022 *Appl. Phys. Lett.* **120** 212103

[37] Huang L, Feng Q, Han G Q, Li F G, Li X, Fang L W, Xing X Y, Zhang J C and Hao Y 2017 *IEEE Photon. J.* **9** 1

[38] Hu W, Li S Y, Hu Y J, Wan L Y, Jiao S J, Hu W G, Talwar D N, Feng Z C, Li T, Xu J H, Wei L M and Guo W 2021 *J. Alloys Compd.* **864** 158765

[39] Wang Y, Li J, Zhang T, Wu W, Li W, Yao Y, Wang Z, Feng Q, Zhang Y, Zhang J and Hao Y 2024 *Appl. Phys. Lett.* **124** 072105

[40] Vo T H, Kim S, Kim H Y, Park J H, Jeon D W and Hwang W S 2024 *Mater. Sci. Semicond. Process.* **173** 108130

[41] Xiang X Q, Li L H, Chen C, Xu G W, Liang F Z, Tan P J, Zhou X Z, Hao W B, Zhao X L, Sun H D, Xue K H, Gao N and Long S B 2023 *Sci. China Mater.* **66** 748

[42] Yu T J, Pan Y B, Yang Z J, Xu K and Zhang G Y 2007 *J. Cryst. Growth* **298** 211

[43] Rafique S, Karim M R, Johnson J M, Hwang J and Zhao H 2018 *Appl. Phys. Lett.* **112** 052104

[44] Saha S, Meng L, Feng Z, Anhar Uddin Bhuiyan A F M, Zhao H and Singisetti U 2022 *Appl. Phys. Lett.* **120** 122106

[45] Yang T H, Fu H, Chen H, Huang X, Montes J, Baranowski I, Fu K and Zhao Y 2019 *J. Semicond.* **40** 012801

[46] Baliga B J 2019 *Fundamentals of Power Semiconductor Devices* (Cham: Springer International Publishing)

[47] Ma H L and Su Q 2014 *Acta Phys. Sin.* **63** 116701 (in Chinese)

[48] P. Sundaram P, Liu F, Alema F, Osinsky A, Jalan B and Koester S J 2023 *Appl. Phys. Lett.* **122** 232105